Liquid ordering induced heterogeneities in homogeneous nucleation during solidification of pure metals

Avik Mahata^a, Tanmoy Mukhopadhyay^{b,c}, Mohsen Asle Zaeem^{d,*}

^a School of Engineering, Brown University, Providence, RI 02912, USA

^b Department of Engineering Science, University of Oxford, Oxford, OX1 3PJ, UK

^c Department of Aerospace Engineering, Indian Institute of Technology Kanpur, Kanpur, India

^d Department of Mechanical Engineering, Colorado School of Mines, CO 80401, USA

*Corresponding author.

E-mail address: zaeem@mines.edu (Mohsen Asle Zaeem).

Abstract

Homogeneous crystal nucleation is prone to formation of defects and often experiences heterogeneities, the inferences of which are crucial in processing crystalline materials and controlling their physical properties. It has been debated in literature whether the associated heterogeneities are an integral part of the homogenous nucleation. In this study by integrating a probabilistic approach with large-scale molecular dynamics simulations based on the most advanced high-temperature interatomic potentials, we attempt to address the ambiguity over the sources and mechanisms of heterogeneities in homogenous nucleation during solidification of pure melts. Different classes of structured metals are investigated for this purpose, including face-centered cubic aluminum, body-centered cubic iron, and hexagonal close-packed magnesium. The results reveal, regardless of the element type or the solidified crystal structure, that the densification process of liquid metals is accompanied by short-range orderings of atoms prior to the formation of crystals, controlling the heterogeneities during homogenous nucleation.

Keywords: Homogeneous nucleation; Heterogeneity; Solidification; Metals; Molecular dynamics simulation; Probability density.

1. Introduction

Solidification of materials is unquestionably one of the most important aspects of several manufacturing processes. Specially, the process of solidification in metals and alloys commonly occur through crystal nucleation, and the process of crystallization plays a major role in processing of metals and controlling their properties [1, 2]. Crystallization in metals generally happens through nucleation, and the nucleation pathways are classified as homogenous or heterogeneous nucleation, depending on how the process of solidification (liquid to solid transformation) gets affected by inherent homogeneities or foreign impurities. The homogenous nucleation can only occur in an ideal condition when the thermal fluctuations can cause self-assembly of the solid particles in the liquid phase. On the other hand, a heterogeneous nucleation is generally believed to require an impurity as the nucleating agent. The observation of nucleation is extremely difficult and so far only a handful of indirect observations are made by various methods such as high energy X-ray and neutron scattering, transmission electron microscopy etc. [3-10]. The liquid atoms arrangement near the substrate (nucleation sites) was popularly reported in recent years for solid-liquid interface in Al-Si by Howe et al. [3]. Similar observation was also performed on for Al-Al₂O₃ [4, 6, 11], Si-AuSi [5], Cu-Zr-Al alloys [12] solid-liquid interfaces that provide insight in the heterogeneous nucleation behavior which dominated by the competition between the liquid layering and the stochastic formation of the nuclei due to the energy fluctuations in the liquid Al. Although there has been tremendous progress in electron microscopy, the observation of formation of nuclei in metallic system remains unrealistic. Computational techniques like MD simulation can bridge the gap by simulating the entire nucleation process.

As the observation of homogenous nucleation is not possible, there has been ambiguity about the process of heterogeneity in homogenous nucleation. The root of this discussion goes back to the work by Liu et al. [13], where they proposed that any nucleation observed under gravity is most likely to have heterogeneities and should be considered a heterogeneous nucleation. It was also theorized that the heterogeneous nucleation in fact dominates the solidification process at a lower supersaturation, while at a very high supersaturation the heterogeneous particles have a weak interaction with the dominant nucleating phase. As a result, the primary kinetics of nucleation is assumed to be imposed by the primary crystalline phase, which this process is often mistakenly considered as a homogenous nucleation. The issue of heterogeneity in homogenous nucleation remains an ambiguous issue till date.

As the real time observation of nucleation in a metallic system has never been done, various theoretical or computational tools such as classical nucleation theory (CNT) [14, 15], density function theory (DFT) [16], molecular dynamics (MD) [17, 18], Monte Carlo (MC) [19, 20], phase-field [21-23], and cellular automata[24] have often been used to study the nucleation process in solidification of metals. Each of the tools has its advantages and disadvantages for simulating homogenous or heterogeneous nucleation, but in fact other than MD, none of the tools can capture the time and length scales of a nucleation process.

The work by Granasy et al. [25] using DFT and phase-field crystal modeling showed a twostep process for homogenous nucleation from the melt of bcc metals (e.g., Fe); they showed that at first a dense amorphous precursor forms, and then the crystalline phase appears via heterogeneous nucleation within the dense amorphous precursor cluster. This study indicated the presence of various secondary phases such as fcc, hcp, icosahedral (ico) utilizing bond order parameter at the metastable stages of nucleation from the melt to the final solid state of bcc metals. Another effort utilized large scale atomistic simulations to study homogenous crystal nucleation phenomena in solidification from liquid Fe [26]. The heterogeneity in homogenous nucleation was theorized by capturing ico atoms as precursors in solidification from Fe melt. This study also proposed that ico rich areas form around the initially formed larger nuclei/grain, and in the later stages of nucleation, smaller nuclei (also referred as satellite grains) form inside the ico rich areas. Although a billion atom MD simulation was completed for this study, a Finnis-Sinclair (FS) interatomic potential [27] was used for the simulation, which predicts the melting point of Fe to be 2,400 K, whereas the experimental melting point of Fe is ~1,811 K. Subsequently, this deviation resulted in an inaccurate prediction of solid-liquid co-existence properties, and the conclusions made by this work are influenced by the inaccuracy of the interatomic potential. Another MD simulation work [28] showed a concealed short range ordering in supercooled liquid suggesting an intimate link between crystallization and glass transition; this work concluded that the supercooled liquid is fundamentally heterogeneous, and in other words the homogeneous nucleation may essentially be heterogeneous. However, the study was limited to imaginary hard sphere solid-liquid instead of a realistic example of metallic elements. Overall, none of the previous studies have universally addressed the heterogeneity issues in homogeneous nucleation during solidification of different metallic systems.

We aim to provide comprehensive and unified insights on the sources of heterogeneities in homogenous nucleation process during solidification of different pure metallic systems considering fcc (Al), bcc (Fe) and hcp (Mg) crystalline metals. We implement the second nearest neighbor

modified embedded atom method (2NN-MEAM) to accurately predict the homogenous-heterogeneous nucleation phenomena during solidification by large scale MD simulations. The interatomic potentials utilized in this work have been fully investigated for the low and high temperature properties as well as the solid-liquid coexistence properties of the metals showing results comparable to experiments [29-31]. The initial crystalline phases in a solidifying metal can be easily observed by using the common neighbor analysis (CNA) method [32], however, CNA can only detect perfect crystalline structures. Crystal orientation analysis is used to further observe heterogeneities in solidification of pure metals. To capture the underlying mechanism causing heterogeneities in homogenous nucleation of pure metals, we study the probability distribution of the density over the bond order parameters [33] and density. We reveal the inherent heterogeneities during the homogenous nucleation of pure metals in a generically probabilistic framework, considering different types of crystal structures.

2. Methods of study

2.1 MD simulation details

We found that at a temperature close to the melt temperature, a small number of crystalline atoms remain in the simulation box. The nucleation simulations should start with a pure liquid with no solid/crystalline regions. Therefore, in order to find the temperature at which a completely melted simulation box with no crystalline atoms can be achieved in a relatively short simulation time (~150 ps), several simulations were performed by increasing the temperature of the simulation box higher than the melting temperature $(T_{\rm m})$ of each element using 25 K intervals. After 16 intervals, when the temperature reached to 1325 K for Al, we could obtain a completely melted simulation box in ~150 ps. The simulation is continued to 300 ps to make sure the initial melt is properly equilibrated. The CNA of the simulation box for very large time scale is provided in Fig. S1(a). The percentage of amorphous liquid atoms kept increasing with increasing the annealing temperature. Finally, the box had no crystalline atoms at 1325 K. The radial distribution function (RDF, g(r)) of the simulation box was calculated for all the temperatures, which is plotted in Fig. S1(b). There are no long-range peaks at 1325 K. The CNA analysis and RDF plots confirmed that Al was completely melted at 1325 K. We repeated the same procedure for Fe and Mg. To create a completely liquid simulation box, Fe and Mg were equilibrated for 300 ps at 3500 K and 1250 K, respectively. MD simulations of homogenous nucleation from pure Al, Fe and Mg melts were performed in a cubic simulation box with side size of 25, 23 and 29 nm, respectively. The time step for all the solidification simulations was 3 fs (see details in Supplementary Section 4 and Fig. S2). Various details of the simulation sizes have been provided in Table S1. It is worth noting that a previous attempt by atomistic simulation for studying homogenous crystal nucleation from liquid Fe [26] utilized a billion atom simulation. However, to study homogenous or heterogeneous nucleation, utilization of such a large-scale MD simulation is not necessary; several studies produced reliable and comparable results to experimental observations with only thousands to million atom MD simulations [28, 34-37]. In fact, a recent study suggests the influence of the simulation size diminishes when a model size is larger than approximately 2 million atoms [35-39] regardless of the materials system due a convergence effect. It is also important to note that a MD simulation using much less accurate interatomic potential, such as FS potential utilizes several orders of magnitudes less computational power compared to the case of utilizing a more accurate interatomic potential, such as the Modified Embedded Atom Method (MEAM) potential.

The nucleation from the supercooled melt can occur at a temperature as low as 300 K for both Al and Mg. In case of Fe the nucleation does not occur below 800 K. However, at low temperatures, due to the lower kinetic energies of the atoms, the nucleation rate decreases. As we studied the time-temperature-transformation (TTT) diagram for homogenous nucleation of pure Al in our previous work [38], it showed higher temperatures above 0.7T_m, the kinetic energy of the atoms is too high to form stable crystalline structure. This is also true for Fe and Mg, as we observe no crystal nucleation above 1250 K and 700 K respectively. We chose the temperature of supercooled melt in the range of 400-600 K for Al and Mg, and 800-1200 K for the simulations when the nuclei size and nucleation rates are stable. The simulation box was solidified isothermally. The number of simulations performed was 5, 7 and 4 for Al, Fe and Mg, respectively. Then each temperature runs were replicated 5 times, so overall 80 simulations were performed isothermally. Each isothermal simulation was repeated 5 times to evaluate the possible errors. Each of the isothermal simulations was run for a total of 3000 ps (1 million time steps) to simulate the crystal nucleation and solidification. The details of all the simulations are provided in Table S1 of supplementary information. The process of crystallization is shown for Al, Mg and Fe is shown in Fig. S3. Different isothermal temperature solidifications are sown for Mg and Fe are shown in Figs. S4 and S5 respectively. An example of quenching in Mg is discussed in supplementary materials in Section 7, Fig. S6. The detailed quenching simulation for Al is also discussed in our previous work [38]. Different methods of identifying the crystalline solids have been verified with different algorithms such as CNA, centrosymmetry, bond order parameters analysis etc. (Fig. S7), and it was identified that CNA is relatively more reliable to separate the liquid from the solid. The methods and algorithm for the fcc/bcc and hcp crystal structures detection can be found in the work by Faken et al. [32]. To detect the ico and bcc atoms in liquid Fe we can directly use OVITO. We only need to provide a cut off distance determining the structures by CNA for Al/Fe or Mg. The cut-off distance for CNA analysis is taken ~0.85, 1.21 and 1.38 times of the lattice parameters for fcc, bcc and hcp atoms respectively.

We also present one of the sample calculations for identifying the critical nuclei during the solidification of Mg in Supplementary Section 9. The size of a nucleus is taken as the average of the maximum length of the nucleus in three perpendicular directions in Fig. S8. Once the nucleus reached the critical size, the potential energy (Fig. S8(b)) decreases and the solidification and crystallization process proceeds very rapidly. While the solidification occurs, the critical nuclei show different crystal orientations, which we discuss in Section 3.1 for Al melt. A similar difference in orientation is also seen in Fe and Mg (see Figs. S9 and S10). The errors of MD simulations in predictions of the nuclei size, the nucleation rate, and the number of nuclei in the simulation box are determined using 5 different simulations, and the results with the standard deviation are presented in the Supplementary Material, Figs. S11, S12 and S13, and Table S3 for the three metallic systems.

2.2 Interatomic potentials

We utilized MD simulations to study the nucleation process from pure Al, Fe and Mg melts. The second nearest neighbor modified embedded-atom method (2NN-MEAM) [40, 41] was introduced to include the directionality of bonding in covalent materials in the EAM formalism. As a result, MD simulations utilizing 2NN-MEAM potentials predict more accurate outcomes with a very small error compared to experimental data of high temperature properties. We recently tested the 2NN-MEAM interatomic potentials for Al, Fe and Mg developed originally by Lee and Baskes [40] for melting and solidification studies. We showed that the original 2NN-MEAM interatomic potentials for Al [42] and Mg [43] and the modified version of the 2NN-MEAM potential for Fe [29] can predict both low and high temperature properties. The results provided in Table S2 show that 2NN-MEAM MD simulations can accurately predict melting point, solid-liquid interface energy, specific heat, and latent heat of Al, Fe and Mg. For example, the predicted melting point of Al using a 2NN-MEAM MD simulation is 925 K [44], which is in a very good agreement with the experimental value of 934 K. The interatomic potentials also predict the melting point for Fe as 1811

K [44] and for Mg as 924 K [45]. The liquid structure factor and radial distribution function predicted by the Al, Fe and Mg potentials [29, 42, 43] has excellent agreement with the experimental data. The necessary studies for solidification and crystallization studies utilizing the 2NN MEAM potentials have been validated on all three metallic systems. The quantitative studies of maximum number of nuclei during solidification, nucleation rate, critical nuclei size and its comparison to CNT shows the reliability of the potential on studying solidification (see Figs. 1 and 2 in Sections 3.1 and 3.2, respectively). Some previous studies were also extended to larger model of 5-10 million atoms solidification of Al, Fe and Mg [46]. Overall the several tests on melting, solidification and crystallization properties performed for Al, Fe and Mg shows excellent agreement with experimental as well as first principle data. In addition to that we also verified several nucleation related data such as maximum number of nuclei, nucleation rate, critical nucleation has been also calculated with these 2NN MEAM potentials. This makes the 2NN MEAM potentials very credible to study nucleation during solidification of Al, Fe and Mg metallic systems.

2.3 Structural characterization: CNA, bond orientational parameters

CNA was used to distinguish the crystalline atoms from those that belong to the liquid. However, CNA only detects the purely fcc/bcc or hcp crystalline phases, but it is not very effective for detecting the intermediate crystal structures or any other types of ordering. Thus, we applied bond order parameter to analyze the structure of the nuclei. CNA needs a reference frame such as 12 neighbors for fcc/hcp and 8 neighbors for bcc. Steinhardt order parameters are independent of the specific crystal structure and do not require the definition of a reference frame. It is provided by the following algorithm based on spherical harmonics [33, 47]. The complex vector $Q_{lm}(i)$ of particle i can be defined as shown in Eq. (1):

$$Q_{lm}(i) = \frac{1}{N_b(i)} \sum_{j=1}^{N_b(i)} Y_{lm}(r_{ij}).$$
 (1)

where, $N_b(i)$ is the number of nearest neighbors around an atom i, l is a free integer parameter, m is also an integer that runs through m = -l to m = +l. The functions $Y_{lm}(r_{ij})$ are the spherical harmonics and r_{ij} is the vector from particle i to j. As the main goal for the bond order analysis is to differentiate between solid (amorphous, crystalline or semi-solid) and liquid, this criterion should be sufficient. If the particle is connected to a smaller number of particles, then it will be

considered as a liquid-like particle. Using this criterion to distinguish solid-like from liquid-like particles one can accordingly search for clusters of connected solid-like particles.

The above-mentioned procedure is quite efficient in distinguishing solid and liquid-like atoms, but unlike CNA it doesn't actually determine the crystal structures. A set of parameters holds the information of local structures, called the Steinhardt order parameters, which are defined as

$$Q_{l}(i) = \sqrt{\frac{4\pi}{2l+1}} \sum_{m=-l}^{l} |Q_{lm}(i)|^{2} . \tag{2}$$

Depending on the choice of l, bond order parameters give different values as the sensitivity of the parameters differs for different crystal symmetries. Different approaches based on these bond order parameters were developed to analyze the structure of the crystalline nucleus during the freezing event. Especially Q_4 and Q_6 are often used as they are a good choice to distinguish between cubic and hexagonal structures [28, 48]. It can be noted that at the zero temperature (without thermal noises) the simple cubic lattice has $(Q_4, Q_6)_{\rm sc} = (0.764, 0.354)$, the body-centered cubic lattice has $(Q_4, Q_6)_{\rm bcc} = (0.036, 0.511)$, the fcc has $(Q_4, Q_6)_{\rm fcc} = (0.191, 0.574)$, the hcp has $(Q_4, Q_6)_{\rm hcp} = (0.097, 0.485)$, and the icosahedral symmetry gives $(Q_4, Q_6)_{\rm ico} = (0, 0.663)$ [48].

3. Results and discussion

3.1 Comparison with classical nucleation theory

In recent homogenous-heterogenous nucleation studies based on MD simulation utilized one billion atoms [49], which indeed studied the growth of grain instead of the actual nucleation process. The study by Shibuta et al. [49] mentioned that the term "grain" is not conceptually different than a solid nuclei in simulation cell, which is probably not a correct assumption to understand the nucleation. The grains form at much later stages when the simulation box is solidified in most part and the nucleus forms from the thermal fluctuations inside the melt. The thermal fluctuation may be caused by changing the temperatures of the simulation box (homogenous) or by adding a second phase which creates more nucleation sites (heterogenous). Thus, the nucleation and grain formation/growth are two different stages of solidification, which has been discussed in our previous work on homogenous nucleation of Al [50]. We discussed about the nucleus size and nucleation rate to justify that almost 25 nm³ simulation boxes with 1 million atoms are sufficient for understanding the heterogeneity in homogenous nucleation. Critical nucleus size is the focal point of the

solidification of the metallic metals. We have showed the steps to identify the critical nucleus size by determining the stable size of the solid cluster in our previous work [50]. The critical nucleus size is compared with the results from Classical Nucleation Theory (CNT) for Al, Fe and Mg. If the results of MD from a million-atom simulation are close to the theoretical results, then this would indicate an optimum size for understanding the nucleation mechanism. CNT provides some detailed insights on the homogeneous nucleation process such as the critical temperature for nucleation and the critical nucleus size. CNT suggests that there is a free (activation) energy barrier, W^* , for formation of solid nucleus with a critical size of r^* . The nucleation typically happens when the probability of energy fluctuation is sufficient to overcome the activation barrier. The probability of energy fluctuation is given by the Arrhenius type equation and the rate of homogeneous nucleation is [51-54],

$$I = I_0 \exp\left(-\frac{\Delta G_{\text{Homo}}}{k_{\text{B}}T}\right) \tag{1}$$

where T is the temperature, $k_{\rm B}$ is the Boltzmann constant, and I_0 is a coefficient that depends on temperature and the interface free energy, $\sigma_{\rm SL}$ [54]. $\Delta G_{\rm Homo}$ is defined by [55],

$$\Delta G_{\text{Homo}} = \left(\frac{16\pi}{3} \frac{\sigma_{\text{SL}}^3}{(\Delta G_{\text{V}})^2}\right) \tag{2}$$

where $\Delta G_{\rm V}$ is the difference between the free energies of liquid and solid crystal per unit volume. If the change in molar heat capacities is constant, $\Delta G_{\rm V}$ according to Hoffman is equal to $\Delta H_{\rm m} \left(T\Delta T/T_{\rm m}^2\right)$ [56, 57], where ΔT is the undercooling ($\Delta T = T_{\rm m} - T$), and $\Delta H_{\rm m}$ is enthalpy of melting. By combining Eqs. (1) and (2), the homogeneous nucleation rate becomes

$$I = I_0 \exp\left[\left(-\frac{16\pi\sigma_{\text{SL}}^3 T_{\text{m}}^4}{3k_{\text{B}}(\Delta H_{\text{m}})^2}\right) \frac{1}{T^3(\Delta T)^2}\right] = I_0 \exp\left(-\frac{A}{T^3(\Delta T)^2}\right)$$
(3)

where, A is a constant that depends on the solid-liquid interface energy and enthalpy. Eq. 3 also suggests that homogeneous nucleation rate strongly depends on the undercooling or the annealing temperature. The nucleation rate is maximum at the critical temperature. The critical temperature can be derived from Eq. (3) by setting its first derivative to zero. This suggests that the critical temperature for Al is $T_{\rm cr} = \frac{3T_{\rm m}}{5} (\sim 550 \text{ K})$. The critical temperature for Fe and Mg are 1087 K and 560 K. The critical temperatures were mentioned before in Table 1, which is 1100 K for Fe and 500 K for Mg. The calculated critical temperature from MD is $\sim \frac{T_{\rm m}}{2}$. This is clearly a reasonable

estimation considering the proximity to CNT and experimental values of critical temperature of nucleation, which lies between 0.5-0.6 times of the melting temperature [58, 59].

We can also find the critical radius from CNT, which is suggested to be

$$r^* = 2 \frac{\sigma_{\rm SL}}{\Delta G_{\rm V}},\tag{4}$$

We previously calculated $\sigma_{\rm SL}$; the specific free energy of the critical nucleus formation is estimated to be the solid-liquid interface free energy of Al, Fe and Mg as 172.6, 188 and 90 mJ m⁻² respectively. The $\Delta H_{\rm m}$ or the latent heat are 11.50 kJ mol⁻¹ for Al [42], 13 kJ mol⁻¹ for Fe [29] and 10.2 kJ mol⁻¹ for Mg. The atomic volume in solidification is available from isothermal simulation for all the materials at a specific temperature. By utilizing Eq. (2) and considering the normalized temperature for annealing, $T_{\rm normalized} = T/T_{\rm m}$, $\Delta G_{\rm V}$ is calculated for different undercooling temperatures. The calculated critical nucleus size is shown in Fig. S13. Al has a critical size between 1.25 to ~4 nm (Fig. 1(a)), whereas the Fe has the critical size between 0.95 to 1.4 nm (Fig. 1(b)). As shown in Fig. 1(c), the critical radius of Mg increases from 1.15 nm to 3.75 nm with the increase in undercooling temperature.

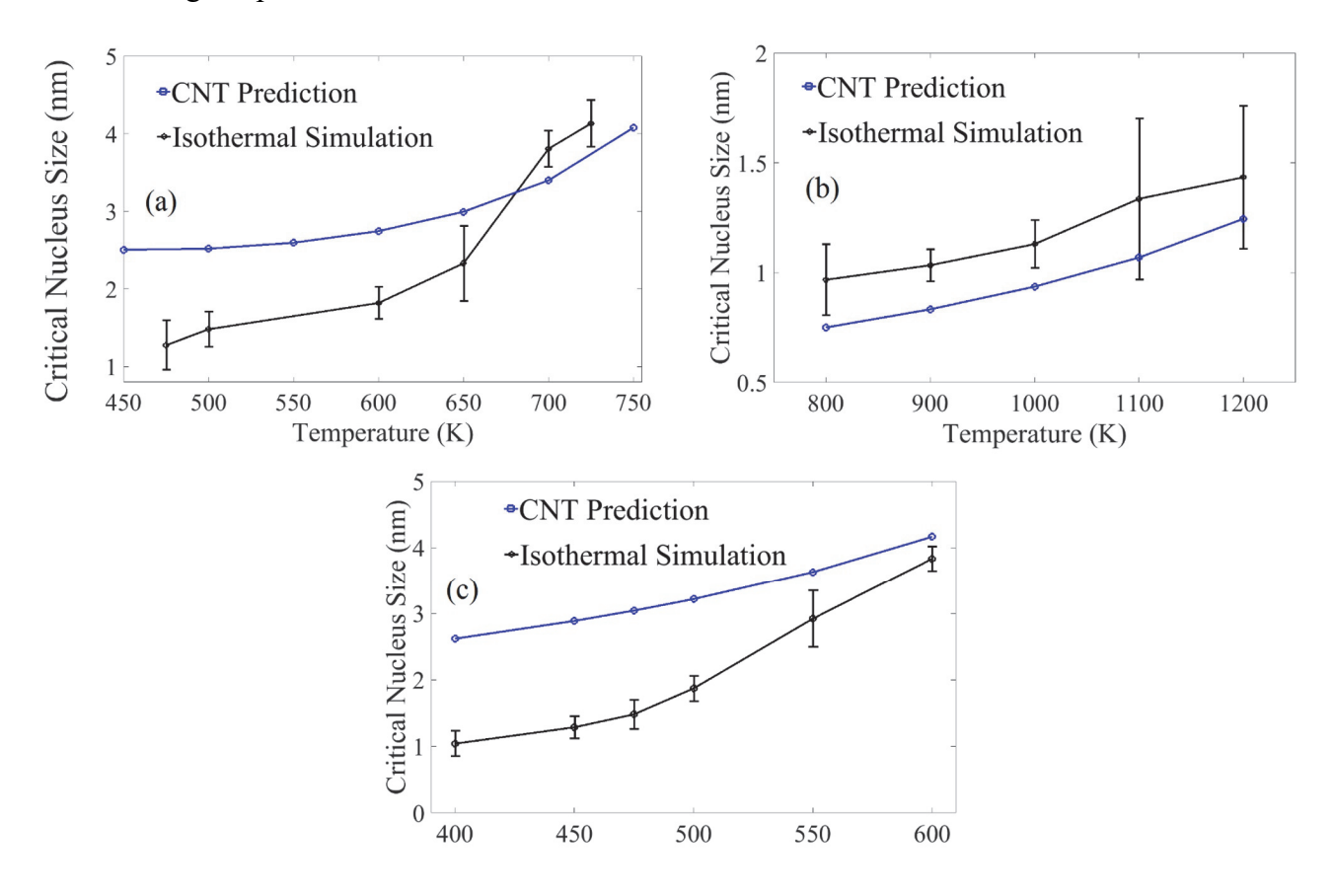


Fig. 1. Critical nucleus size calculated by CNT at different temperatures is compared with the results of MD simulation for (a) Al, (b) Fe and (c) Mg.

As shown in Fig. 1, CNT either overestimates (Al and Mg) or underestimates (Fe) the critical size at higher undercooling or lower annealing temperature. The difference between CNT and MD at lower undercooling temperatures can be explained by Eq. (4). To calculate the critical nucleation size at different annealing (or undercooling) temperatures by Eq. (4), σ_{SL} at the melting point is used in a similar way as most of the other works in Refs. [60-62]. This means the numerator of Eq. (4) is kept constant for calculating the critical size nucleus at different temperatures. At the same time, the free energy difference between the liquid and solid crystal per unit volume gradually increases. As a result, the critical nucleus size predicted by CNT tend to increase with increasing temperature. However, physically σ_{SL} reduces with a lower the annealing temperature (or a higher undercooling) [63, 64]. Therefore, the numerator of Eq. (4) should also decrease with lowering the annealing temperature, making the critical size predicted from CNT to become much closer to the MD simulation data for Al and Mg. The nucleation in Fe is slightly different than Al and Mg, as the bcc Fe forms with an intermediate ico atoms (see Section 3.4). The solid-liquid interfacial energy of Fe is also higher than both Al and Mg (see Table S2). Therefore, the CNT prediction underestimates the critical nucleation size due to the gradual formation of bcc Fe atoms and the higher interfacial energy. Overall the critical nucleus size, predicated for the three elements, remains well within the CNT prediction, especially at high annealing temperatures (or low undercooling). Thus, by determining all the different nucleation parameters such as detection of critical nucleus, maximum number of critical nuclei, nucleation rate, critical nucleus size, it can be concluded that 1 million atoms (~25 nm³) simulation is optimum to study the fundamental nucleation mechanism.

3.2 Rate of nucleation

The rate of nucleation is defined by the amount of independent critical nuclei present in a unit area and time. In the case for our simulations, we count the independent critical nuclei in each timestep. It is plotted against the time and converted to bulk unit of m⁻³ s⁻¹. The simulation boxes containing one million atoms are sufficient for estimating the nucleation rate. The rate of nucleation is influenced by solidification temperature. The increasing number of nuclei is plotted against time in Fig. 2(a-c) for Al, Fe and Mg respectively. The slope in Fig. 2 changes with changing undercooling temperatures. This happens due to slower or faster dynamics of the atoms at lower or higher undercooling temperatures respectively. It is also noticed from Fig. 2 that the nucleation rate

does not monotonously increase or decrease. For 300 and 600 K in Fig. 2(a), the slopes are lower than the slopes at 450 K or 550 K. This essentially indicates that there is a critical temperature where the nucleation rate can be maximum. For Al, it is 475 K, which has been identified in our previous publication [50].

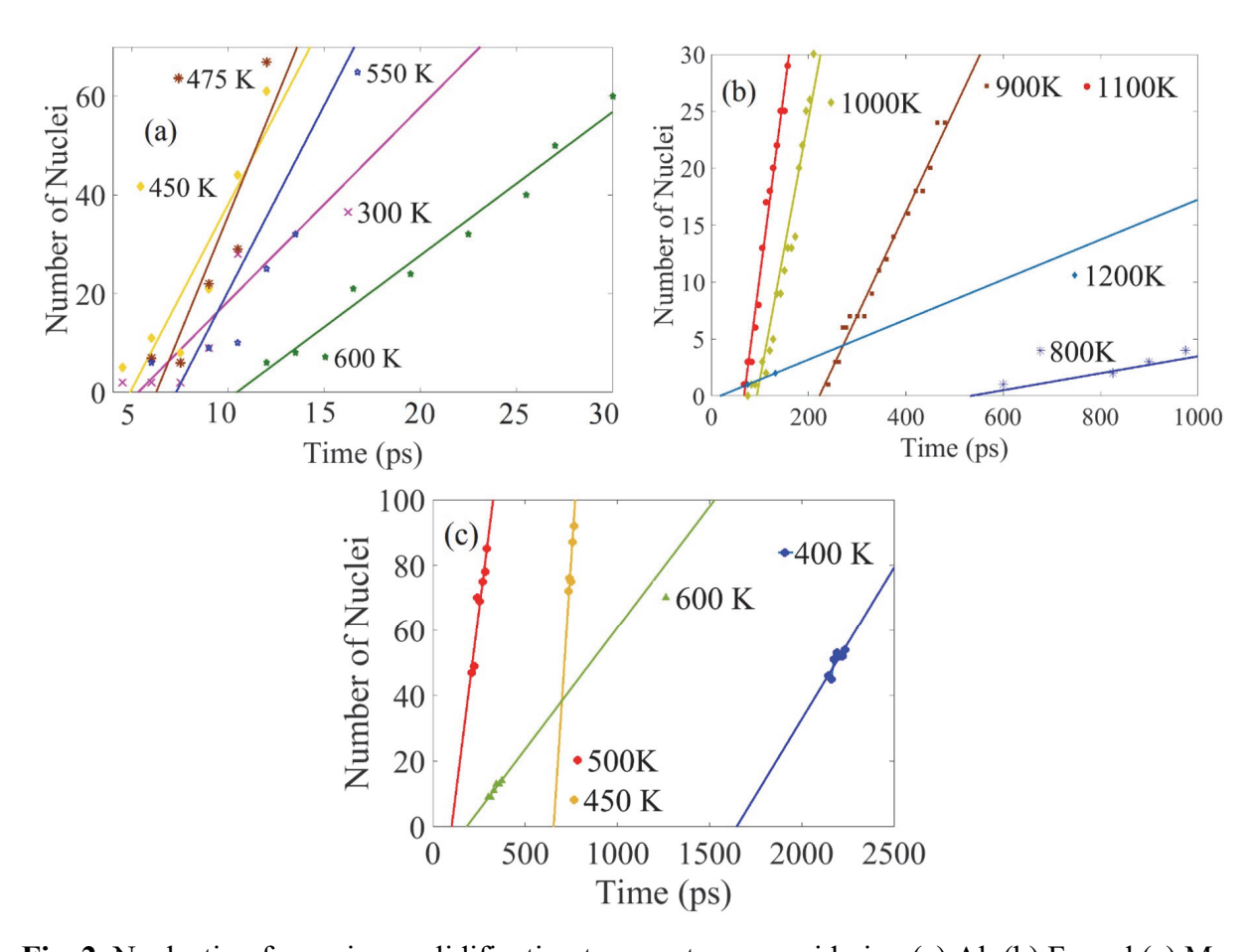


Fig. 2. Nucleation for various solidification temperatures considering (a) Al, (b) Fe and (c) Mg.

For Fe the nucleation rate is higher in 1000 K and 1100 K (Fig. 2(b)) than it is in 800 K or 1200 K. Mg also follows a similar pattern where the nucleation rate is higher in an intermediate stage between 400 K and 600 K (Fig. 2(c)).

The rate of nucleation is calculated for all three crystal structures (Table 1), all of which remain within 10^{33} - 10^{35} m⁻³ s⁻¹. The typical nucleation rate for homogeneous nucleation of a pure metal near the critical temperature has been estimated previously from experiment to be in the order of 10^{30} and 10^{40} m⁻³ s⁻¹ [1, 65, 66], which is comparable to our MD results. The maximum (critical) nucleation rate is observed at 475 K which is $\sim T_{\rm m}/2$, where $T_{\rm m}$ is the melting temperature of Al (925)

K). A detailed discussion is provided in our previous work [50]. The critical temperature for Fe is at 1100 K when the nucleation rate is 2.7×10^{34} m⁻³ s⁻¹. The maximum nucleation rate of 1.7×10^{34} m⁻³ s⁻¹ is observed at 500 K. The critical temperature for both Fe and Mg are also $\sim T_{\rm m}/2$. The discussion on nucleation rate on various single elements gives a clear indication that the millionatom simulation with box size of almost 25 nm³ is sufficient to study the characteristics of homogenous nucleation.

Table 1. Nucleation rates of different materials at different annealing temperatures. The statistical error is estimated by obtaining the slopes for 5 different simulations of each annealing temperature.

Materials	Temperature	Nucleation Rate
Materials	(K)	$(10^{35}\mathrm{m}^{-3}\mathrm{s}^{-1})$
	400	4.00±0.13
Al (fcc)	450	4.48 ± 0.08
	500	5.32 ± 0.05
	600	3.51±0.01
	900	0.18±0.03
Fe (bcc)	1000	0.2 ± 0.05
	1100	0.27 ± 0.09
	1200	0.15 ± 0.01
Mg (hcp)	400	0.06±0.03
	450	0.15 ± 0.02
	500	0.17 ± 0.07
	600	0.05 ± 0.02

3.3. Visualization of crystalline atoms during nucleation

CNA analyses detect that the nuclei within the melt are composed mostly of fcc atoms for Al, bcc atoms for Fe and hcp atoms for Mg. CNA analyses also show that the Al and Mg nuclei form twin boundaries (TBs) (see Fig. S3 in supplementary information). The simultaneous formation of the primary crystal structure and TBs with a secondary crystal structure within a single nucleus shows a sign of heterogeneity in homogenous nucleation from pure Al and Mg melts. The observation of TBs having a secondary crystal structure in Al and Mg is consistent with the earlier studies[35, 37, 38], and in general, the formation of TBs in homogenous nucleation from pure

metallic melts has been reported in various experimental and computational works [67-69]. However, the CNA analysis cannot identify any TBs in Fe, because TBs in Fe do not have a different crystal structure than bcc Fe. Also, CNA is unable to track any ordering of atoms before the crystallization is complete[70] and any orientation or directional differences. Thus, in the following, we analyze the crystal orientation (OR) of the nucleating solid atoms to detect other signs of heterogeneities during homogenous nucleation. The orientation of atoms can be studied by utilizing the OVITO modifier called Polyhedral Template Matching (PTM) method [70]. PTM modifier is capable of calculating the local lattice orientation for atoms that match one of the structural types (e.g., fcc, bcc, hcp, etc.). In Fig. 3, the primary fcc crystal structure of nuclei from Al melt is identified by CNA analysis, and the OR analysis shows the orientations of grains from the principle axes (i.e., x, y, z) of the simulation box. For the coloring purposes, we only considered the orientation from the principle Z axis. The coloring scheme is applied in Open Visualization Tool (OVITO) [71] software, and the details can be found in an article by Larsen et al. [70]. GBs (Grain Boundaries) and TBs separate the grains with different orientations, but generally, the TBs separate the grains in a symmetrical manner.

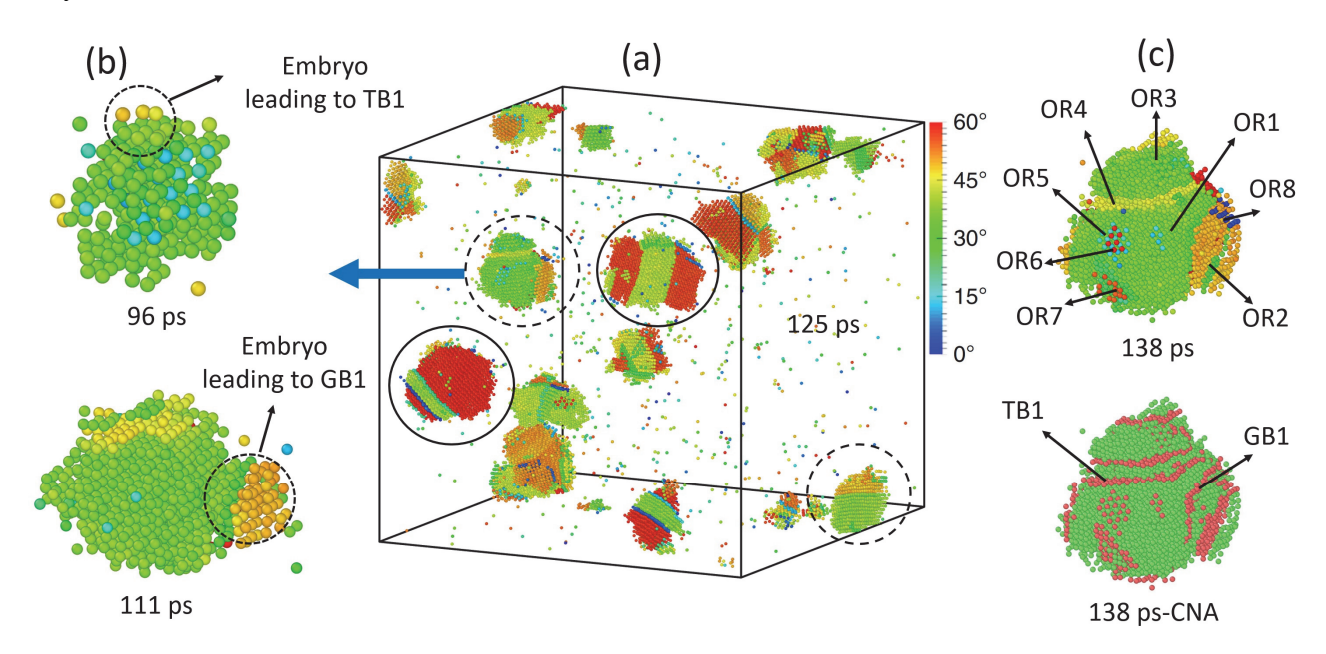


Fig. 3. Visualization of heterogeneity in homogenous nucleation. (a) The complete simulation box at an intermediate stage of nuclei formation from Al melt. The solid circles show nuclei with TBs, and the dotted circles show nuclei where embryos form as precursors for TBs/GBs. (b) Two time steps showing embryo formation on top and side of an initially formed nucleus. (c) Formation of TBs and GBs ii the initial nucleus in (b); the orientations are shown in the top image by orientation-coloring, and CNA method shows two crystal types in the below figure. All the red atoms with hcp stacking are TBs or GBs, or stacking faults that later transform to TB or GBs. Some amorphous GBs are not shown and they can be observed from the orientation coloring.

Visualization of the crystal nucleation by the CNA methods gives a clear indication of how the secondary phase forms during nucleation from the melt of a single element. With the simple observation of TBs/GBs with CNA analysis, at least two different phases within a nucleus of pure Al and Mg are detected, which can contribute to the heterogeneities in homogenous nucleation. TBs in Al have a hcp phase and are basically special GBs, where the atoms in both side of the twins have a mirror symmetry. Both TBs and GBs similarly contribute to the heterogeneity. At growth we observe the heterogeneities caused by stacking faults mediated twins are shown in Fig. 3(c) for Al and Fig. S9 for Mg. Significantly lower stacking fault energies at higher temperatures imply a great tendency to form stacking faults, which turn into TBs while solid atoms gather around the stacking faults in the process of crystallization during nucleation from melt. As we trace back the process in Fig. 1(b), we identify that both TBs and GBs has a common origin of embryo formation. By the definition of heterogeneous nucleation, an embryo forms at the solid-liquid interface of the previously formed nucleus. The interface turns into a stacking fault which later forms either a TB or a GB, depending on the orientations of the opposite sides of the once solid-liquid interface. As shown for two time steps in Fig. 3(b), the formation of atoms having a different orientation than the initial nucleus is similar to formation of an unstable embryo, which eventually becomes stable and a part of the initially formed nucleus, and in this process a TB or GB forms, Fig. 3(c). In Fig. 3(b), the heterogeneous nucleation process of a nucleus from Al melt shows formation of two embryos of different orientations. The embryo on the top eventually forms a TB (denoted as TB1), and one of the right forms a GB (denoted as GB1). In Fig. 1(c) at 138 ps, there are eight different orientations for the atoms within the nucleus, so in addition to the initial cluster of solid atoms, the nucleus gathers various different embryos from the liquid Al. At the same time step at 138 ps, if we analyze the nucleus with CNA method by the types of crystalline atoms, we see several parts of this nucleus is separated by stacking faults, TBs or GBs having a different crystal structure (hcp). Stacking faults which are precursors to TBs are detected as hcp in Al atoms. Some GBs may also show a hcp configuration in the early stages of solidification. By comparing the orientation map (top, Fig. 1(c)) and the CNA map at 138 ps (bottom, Fig. 1(c)), we can identify several embryos (with different orientations) separated by TBs and GBs within one nucleus that formed during the nucleation process from a pure metallic melt. There are very close similarities in the nucleation process from Al and Mg melts (see Figs. S4 and S9) for nucleation from Mg. In nucleation from Fe melt (see Figs. S5 and S10), the formation process of TBs and GBs are similar to Al and Mg case, however,

it is visually different. More discussions are provided in Section 8 of the supplementary document. Overall the visualization methods show the evidence of heterogeneity in homogenous nucleation, where formation of embryos resulted in origination of TBs and GBs. The visualization methods can only show the evidence of heterogeneity, and they cannot explain the mechanisms leading to heterogeneity, which is the focus of this research.

3.4. Variation of free energy during solidification/crystallization of a single nucleus

GBs or TBs create the separations between grains and ease the process of nucleation, and here we apply the Young's relation[72] for heterogeneous nucleation and study how TBs and GBs influence the free energy during nucleation. The change in free energy will indicate whether the homogenous nucleation gets influenced by any heterogeneity or not. The change in free energy involving GBs (or TBs) can be estimated by Eqn. 4.

$$\Delta G_{\text{Hetero}} = f(\theta) \Delta G_{\text{Homo}} = \frac{(1 - \cos \theta)^2 (2 + \cos \theta)}{4} \Delta G_{\text{Homo}}, \tag{4}$$

where, $\cos\theta=1-\frac{\sigma_{GB}}{\sigma_{SL}}$ comes from the Young's relation [74] and σ_{GB} (σ_{TB}) is the GB (TB) energy and σ_{SL} is the solid liquid interface energy. Now if the change in the free energies in homogenous nucleation and heterogeneous nucleation are ΔG_{Homo} and ΔG_{Hetero} , respectively, then in general, the change in free energy of crystal nucleation can be approximated by Eq. (4) and if $f(\theta)$ is less than 1, then there is heterogeneity in homogenous nucleation. The free energy of formation of one crystalline nucleus is then reduced by the fact that the amorphous atoms around TBs or GBs can easily crystallize compared to the spontaneous crystallization in rest of the simulation box within non-structured atoms. In simulations, we get the angles similar to the one we assumed for determining $f(\theta)$. In Fig. 4(a), a TB divides the fcc atoms in an Al nucleus in two different directions with a misorientation of ~122° by (111) tilt axis. Fig. 4(b) shows the formation of a GB with ~109° misorientation in Fe separating two different nuclei by (110) tilt axis. In Fig. 4(c), Mg nuclei with stacking faults are separated by GBs.

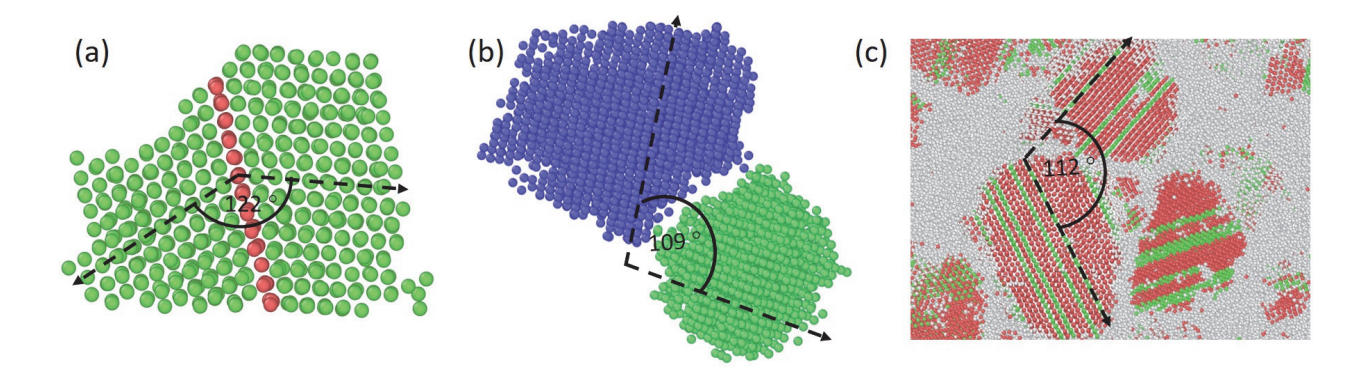


Fig. 4. Twin boundaries between nuclei. Snapshots showing the atomic configuration at the initial stages of nuclei formation. (a) Al nuclei forms with a TB, and there is 122° angle between atoms on the opposite sides of the TB. The coloring method is CNA, where red atoms are hcp, and green atoms are fcc; (b) Formation of a GB with $\sim 109^{\circ}$ misorientation in Fe; colors show different orientations and (c) Mg nuclei formation with stacking faults and a GB with misorientation angle of $\sim 112^{\circ}$. CAN shows that red atoms are hcp, and green atoms are fcc.

Table 2 shows the calculated values of $f(\theta)$ for all the elements remain less than 1, which suggests that the TBs and GBs are contributing towards the heterogeneity during the homogenous nucleation.

Table 2. The solid-liquid interface free energy, and GB and TB energies of Al, Fe and Mg.

	$\sigma_{\rm SL}({\rm J~m^{-2}})$	$\sigma_{\rm GB}({ m J~m^{-2}})$	$\sigma_{\mathrm{TB}}(\mathrm{J}\;\mathrm{m}^{-2})$	$f(\theta)$
Al	0.17 [44]	0.25-0.3 [75, 76], 0.23	0.08-0.20 [78, 79]	0.61-0.90
Fe	0.19 [44]	0.30 [80]	0.16 [81], 0.135 [82]	0.89, 0.29-0.38
Mg	0.12 [43]	-	0.14±0.05 [83]	0.65-0.81

The primary goal of this paper is to address the possible heterogeneities created during homogeneous nucleation, and this work does not deal with heterogeneous nucleation which requires aid (impurities, surfaces, etc.). Fig. 3 in Section 3.2 shows all the possible visual characteristics we can extract from MD simulation. The TBs and GBs can form due to growth; however, a secondary nucleus can form with different orientations on top of the primary nuclei at the twin or grain boundaries. Similar observation was shown on Fe atoms by Shibuta et. al[49]. Young's equation has been utilized to show the reduction in free energy due to the presence of the twin or grain boundaries. As $f(\theta)$ has fractional values, that definitely helps accelerating the nucleation process. But we only

refer it as heterogeneity in homogenous nucleation rather than heterogenous nucleation. In the later stages of this article we use the short-range ordering that exists before forming any crystalline structure. These short-range orders coexist with the crystalline atoms and liquid. We refer this coexistence of three different phases at liquid and decoupling during the solidification as heterogeneity in homogenous nucleation.

3.3. Heterogeneities Explained by Structural Classification using Bond Order Parameters

The orderings in the liquid atoms can be described by their translational orders, which can be determined from two body correlation functions such as the pair distribution function. Local density correlates well with the pair distribution function, and it can be obtained from Voronoi diagram of particle arrangements (Voronoi tessellation). This is why translational order often obtained from the measurement of local density. However, bond orientational order parameters are more sophisticated and are obtained from many-body correlations rather than two-body translational orders. The local density is inverse of the specific volume, and it is computed in this work via Voronoi analysis utilizing Voro++ code implemented in LAMMPS. The program gives us the volume around each atom and local density is inverse of the volume. In this article, the local density is referred as density and its unit is Å-3.

To characterize different structural orders, we consider the density and the bond orientational order Q_6 parameter plots for specifying the local symmetry (see Section 2.2). Both Q_4 and Q_6 parameters can indicate the structural orders in a system, but without thermal noises the Q_4 parameter for ico atoms is 0. Thus, we utilized the Q_6 parameter in our analysis as it has a positive value for all the crystalline materials. The Q_6 and density (ρ) are studied during all the solidification cases. For analysis purposes, we divide the crystallization process in three distinct regions based on their bond orientational order parameter (Q_6). As from the CNA analysis we are aware of the region where the nucleation happens, we choose a cluster of ~5000 atoms around the first critical nuclei and analyzed at different time steps during the solidification process as shown in Fig. 5. the dotted red rectangle for $Q_6 < 0.3$ represents the atoms that remain liquid or have a short-range order (SRO). Then the region $0.3 < Q_6 < 0.45$ (Fig. 5(a)) is a mixture of crystalline and SRO

The peak of $P(\rho)$ remains within the same range, but the range over Q_6 increases for the short range order atoms (Fig. 5(b)). Finally, when the SRO becomes crystalline fcc and hcp, the range over Q_6 becomes narrow with the peak of probability density much higher than that of SRO, and this signifies that most atoms have been converted to fcc and hcp. For Fe (Fig. 5(d)) and Mg (Fig. 5(f)), the value of Q_6 changes but the same three regions (three dotted rectangles for each case) can be identified.

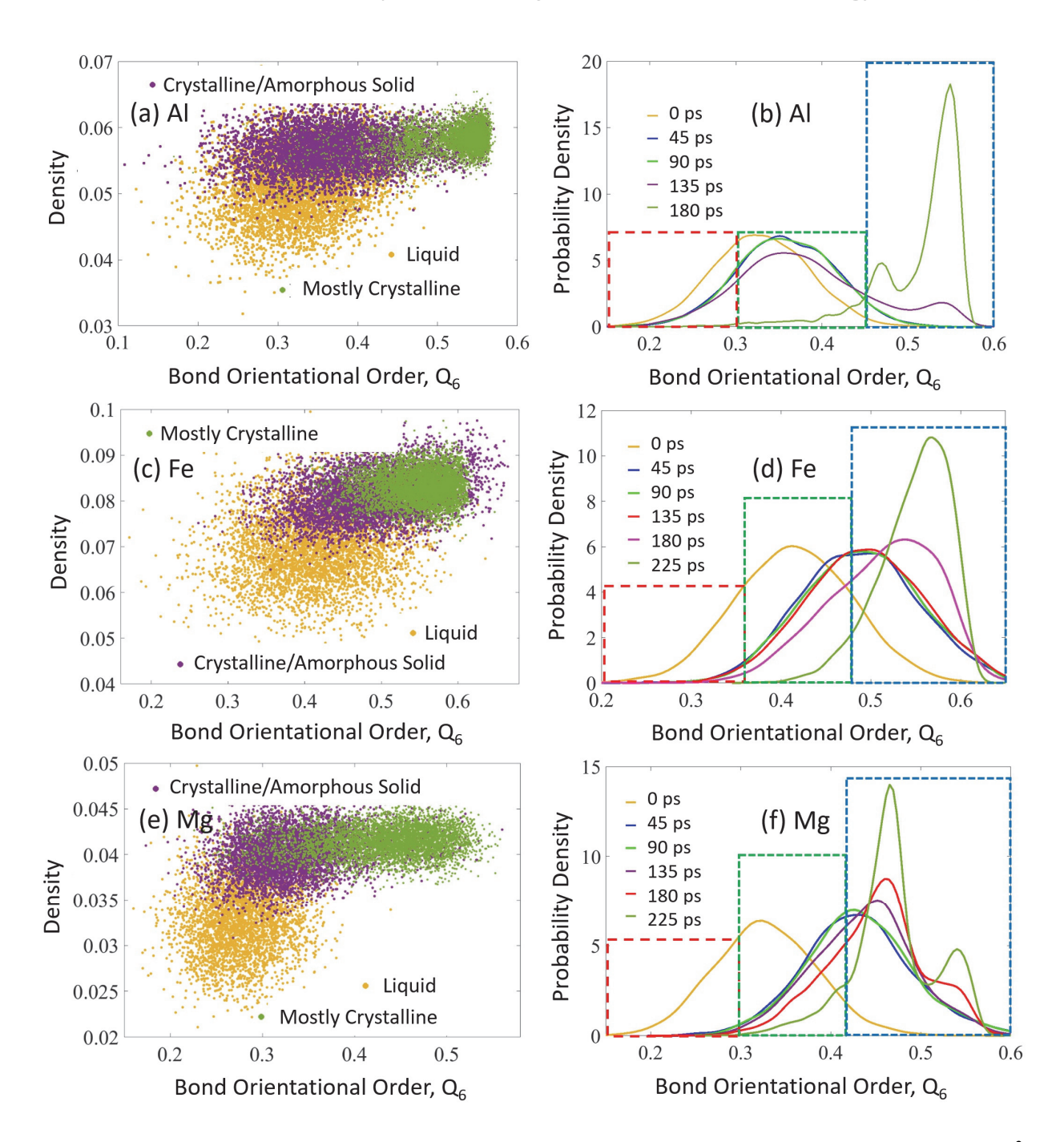


Fig. 5. Density and probability density versus bond orientational order (Q_6). Density (ρ , A^{-3}) versus the bond order parameter for (a) Al at 500 K, (c) Fe 1100 K and (e) Mg 550 K considering the same probability distribution function. The probability density function for bond orientation order parameter Q_6 for (b) Al at 500 K, (d) Fe at 1100 K and (f) Mg at 550 K; the dotted red rectangles show the SRO atoms, the green rectangles indicate the mix or SRO and crystalline atoms, and the blue rectangles indicate crystalline atoms.

Based on the preceding discussions, the process of solidification by nucleation can be referred as a two-step crystallization process: the first step involves the formation of dense

liquid/solid regions, and the second step is the nucleation of the crystal phase inside these dense regions. It is hard to exactly differentiate the solid and liquid regions by any of the existing methods. But the atoms referred to as SRO in the beginning of the solidification can be considered as liquid, and at later stages of solidification those SRO are glassy solids. As shown in Fig. 5 (a), (c) and (e), we can clearly observe the two-step process of crystallization: 1. Densification step where the super saturated liquid forms a dense metastable phase which contains several SRO atoms, and basically in this step the density increases without a significant change in bond order parameter, and 2. The crystallization step where the bond order parameter changes without a significant change in density. Thus, this two step mechanism of crystal nucleation is influenced by both critical fluctuations of thermodynamics quantities and the formation of a dense liquid/solid phase that is thermodynamically stabilized below the critical point. Away from the metastable critical point, such as later stages of the solidification when different crystal nuclei already present in the simulation box, the system was found to crystallize classically in one step, where slight densification and structural orderings happen simultaneously. However, the analysis of bond order parameter can generally indicate that the crystallization in single crystal metallic system is accompanied by several SRO phases which initiate the crystal nucleation phenomena. The SRO phases are the most significant steps that form during the nucleation. As shown in Fig. 6(a) and (b), there are several relatively dense areas all over the liquid Al matrix. The nucleation and growth steps of a nucleus are shown in Fig. 6 using CNA (Fig. 6(c-f)), density (Fig. 6(g-j)), and interatomic distances (Fig. 6(kn)). Although there are several areas that have clusters of atoms with a higher density than the rest of the liquid, it doesn't always form SRO. As shown in Fig. 6(k-n), the interatomic distances have to also change significantly for the nucleation to happen. The process of identifying the first nuclei is discussed in section 9 of the Supplementary Material based on our previous work [38]; it requires a nucleus not to lose any crystalline atoms in the liquid and has a steady increase in size. To fulfill all the conditions, the crystalline nuclei also need to have the bond length similar to the theoretical fcc Al-Al bond length. Crystalline fcc Al atoms have a bond length ~2.8 Å. As shown in Fig. 6(n), the interatomic distances remain close to the theoretical bond length. Therefore, in the two steps of densification and bond order change during the nucleation process, the underlying condition of having a proper bond length for the solid or semi solid clusters must be also satisfied.

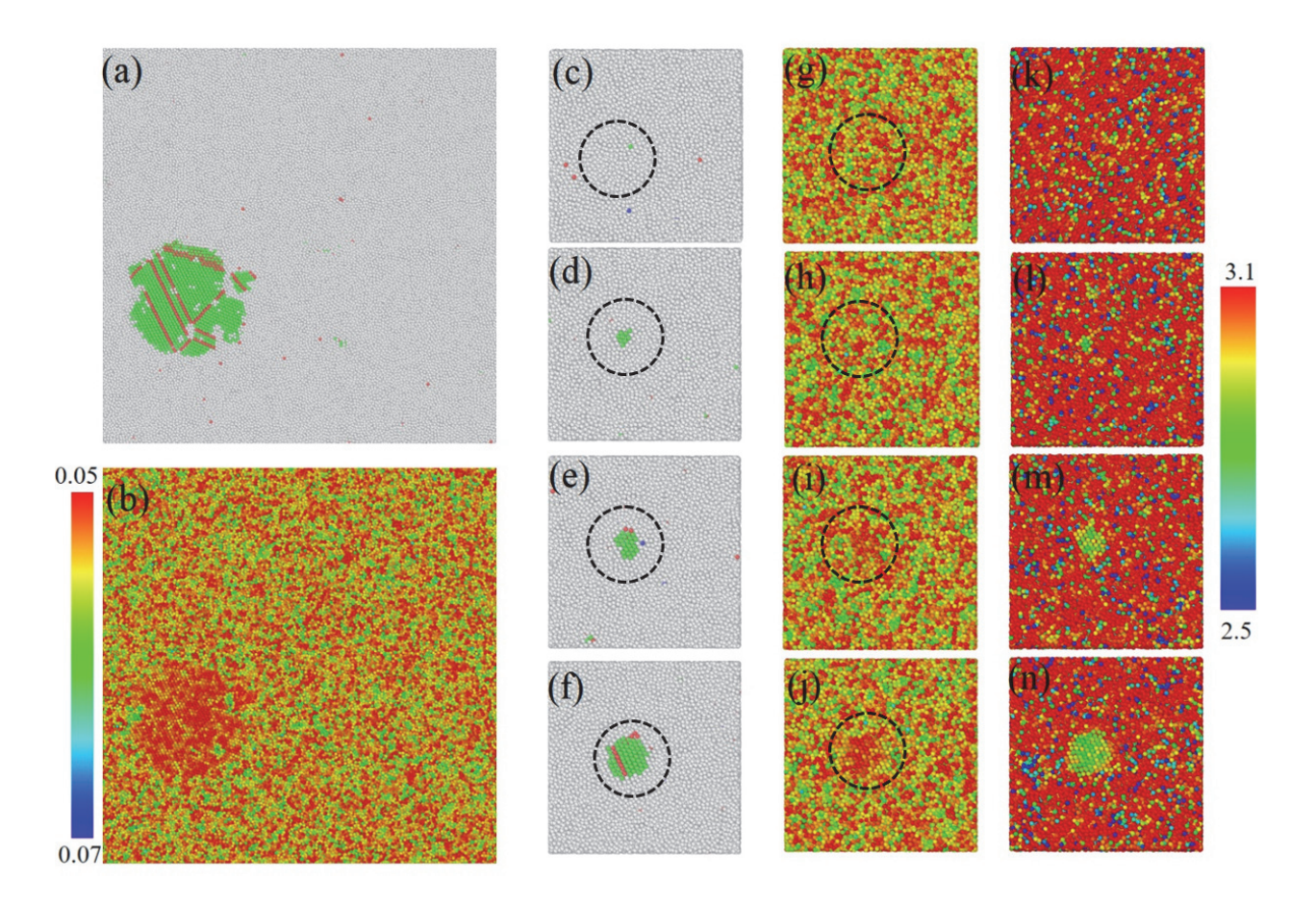


Fig. 6. Densification and crystallization steps in solidification. (a) A nucleus is shown during its growth in isothermal solidification of liquid Al at 500 K at 125 ps by CNA. Red atoms are hcp, green atoms are fcc, and grey atoms are liquid. (b) At the same timestep density is shown for the Al matrix. The area around the nucleus shows higher density. The formation of the first critical nucleus by CNA (Fig. 6(c-f)), density (Fig. 6(g-j)), and interatomic distances (Fig. 6(k-n))) are shown at 10 ps, 25 ps, 50 ps and 75 ps, from top to bottom. The colorbar on the left is for density, and the colorbar on the right is for interatomic distances in Å. The dotted circles show the common neighbor analysis and density of the nucleation sites.

In the context of the heterogeneity in homogenous nucleation, the major identification of heterogeneity can be made from Fig. 5(a, c, e) by looking at the bond order and density during the solidification. The change in density is comparatively much less than the bond order in the stages between liquid (0 ps) and formation of solid (135 ps) (Fig. 5(a, e)). It indicates that the mixture of crystalline and amorphous solids at the intermediate crystalline-amorphous stage (135 ps in Fig. 5(a, e) and 225 ps in Fig. 5(c)) must have interactions and there are interchanges between them. As the crystalline solids possess the minimum energy configuration, most of the amorphous solids eventually transform into crystalline solids. Thus, the amorphous solid atoms can be considered as

precursors for formation of crystalline nuclei for all the crystalline metals. If we consider this amorphous phase as a second phase with respect to the primary crystalline phase, then we can also say that the heterogeneity exists at the same time as the homogenous nucleation starts.

3.4. Formation process of bcc-Fe nuclei

Having analyzed the SRO during the solidification for all the studied metallic elements, here we try to focus on the Fe liquid for its initial structures during solidification. Previously, it was hypothesized that the ico atoms are precursors for formation of the bcc crystalline Fe atoms, and the bcc nuclei are more probable to form in the regions where the ico has a higher density [49]. However, the maximum number of ico atoms is only about 5% at any instant during the nucleation and growth (Fig. 7), and the number of bcc atoms can reach as high as 80% depending on the undercooling temperature. Thus, it is apparently inaccurate to consider ico atoms as precursors for formation of bcc atoms. It should be noted that the number of ico atoms in the simulation box can be influenced by the cut off used to identify them or the algorithm used for identification (see the Methods section). Also, it should be noted that the accurate percentage of ico atoms can be significantly impacted if the interatomic potential used for the MD simulation is not accurate enough for studying solidification.

As shown in Fig. 7(a), during the initial stages of the nucleation (\sim 200-250 ps), the number of both ico and bcc atoms increases in the system. As we look into the detailed structure of the undercooled Fe (Fig.7(b)), it is not necessary to have dense ico atoms for the origination of bcc-Fe nuclei. Considering atoms having $0.3 < Q_6 < 0.45$ possess SRO, instead of the ico atoms, there are a large number of SRO (solid or liquid) atoms in the system before bcc atoms form. The density of the SRO atoms increases in the areas where the bcc-Fe nuclei forms and vice versa. It is worthy to note that although few atoms are detected by CNA algorithm as ico atoms during the solidification, they do not necessarily influence the nucleation process as the number of ico atoms never reach 5% of total atoms in the system. Heterogeneity also comes from the TBs and GBs in Fe nucleation, which is similar to the heterogeneities in homogenous nucleation of Al and Mg. The ico atoms might be considered as an artifact of the visualization algorithms. If other methods such as bond orientational order parameters are utilized, ico atoms may not have any significance on studying the nucleation process.

The parallel comparison of CNA and Q_6 (Fig. 7(c)-(e)) shows nucleation in the initial stages are spontaneous. For the few initial nuclei, the nucleation stays purely homogenous. Once the nuclei grow in size, embryos form on them. As an embryo has a different orientation than the original nucleus, there is an obvious TB or GB between the parent and an embryo, which brings down the free energy and eases the process of nucleation. The heterogeneity in homogenous nucleation originates from the formation of embryo along TBs or GBs. The embryo accelerates the nucleation process. The acceleration in nucleation process can also be attributed to the SROs in the liquid atoms prior to solidification. As long as the visualization and analysis can detect those changes in atomic scale, we can detect the heterogeneity in homogenous nucleation of any metallic systems.

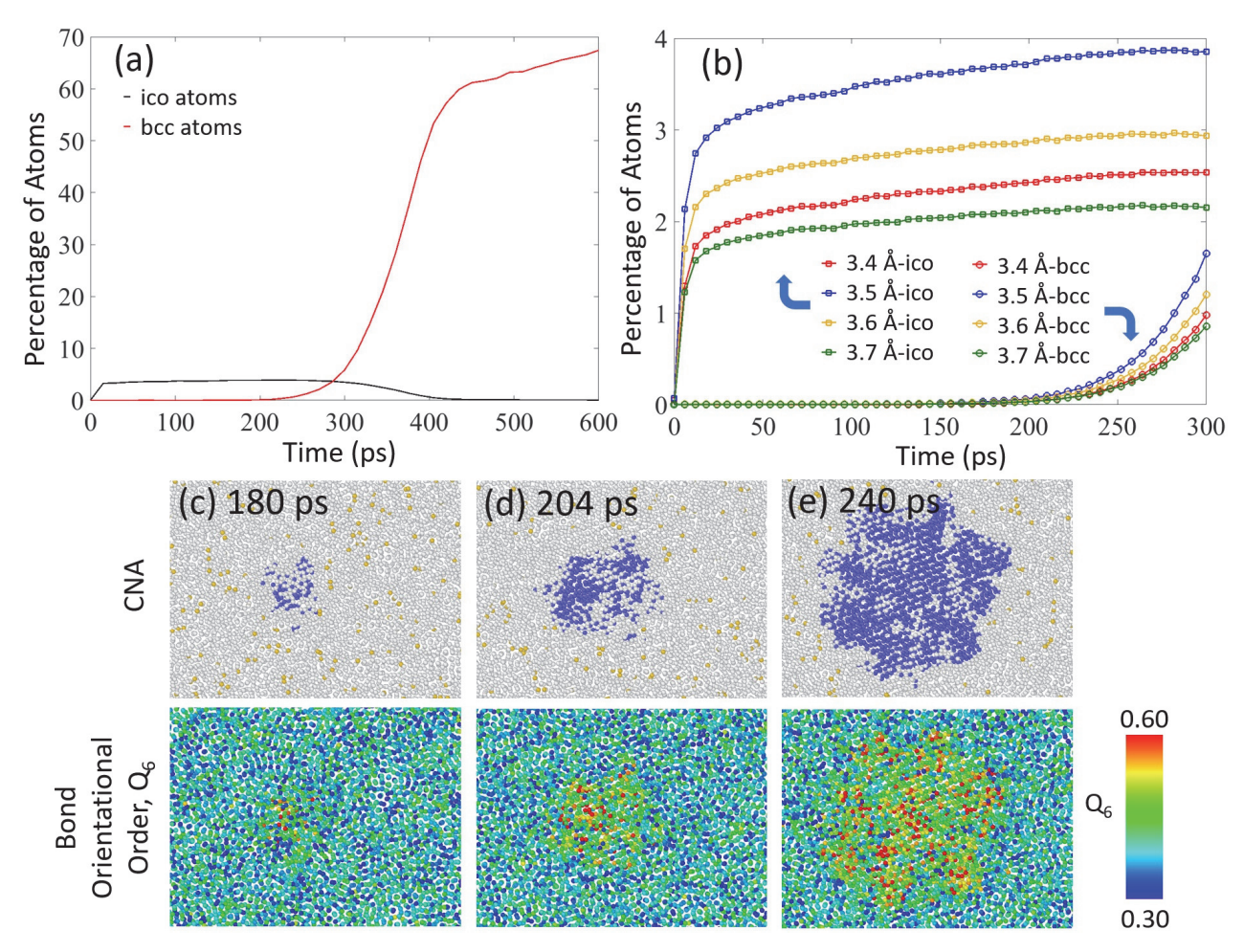


Fig. 7. Time evolution of ico-bcc atoms during solidification. (a) Time evolution of bcc and ico atoms in nucleation of Fe at 1100 K isothermal solidification simulation. (b) Bcc and ico Fe atoms before the formation of critical nuclei. (c)-(e) The CNA and the bond orientational order parameters at 180 ps, 204 ps and 240 ps. In CNA, the white atoms are liquid/amorphous solid, blue atoms are bcc and yellow atoms are ico. Bond order coloring is shown in the color bar.

Besides the aforementioned sources of heterogeneities, if we assume that there might be another origin of heterogeneity from the structures of the semi-crystalline solids that actually contribute towards the nucleation process in the first place, we should also focus on the structural characterization of the atoms during solidification.

3.5. Heterogeneities explained by landau free energy landscape

To further investigate the origins and mechanisms of heterogeneity in homogenous nucleation, we analyzed the joined probability function considering both the density and order parameter. From the perspective of the solidification, it makes sense to investigate the details of whether the nuclei appear in dense precursors or in bond orientational-ordered precursors. The study of "density first" shows the increase of density leads to nucleation[83]. In the case of homogenous nucleation in a metallic system, we define the Landau free energy[84, 85] by taking joint probability of Q_6 and density (ρ) as

$$F(Q_6) = -k_B T \log P(Q_6, \rho). \tag{4}$$

In Eq. (4), $k_{\rm B}$ represents the Boltzmann's constant. Fig. 6 represents the joint probability plot of Q_6 and ρ for Al solidification; a similar behavior for Fe and Mg are observed, please refer to S12 and S13, respectively in the supplementary materials. An interesting decoupling between $P(Q_6)$ and $P(\rho)$ can be noticed, expressing the fact that Q_6 and ρ capture the fluctuations in bond orientational order and mass density independently. This decoupling indicates a two-step nucleation process. At first the density increases, and the liquid atoms comes together and then the cluster of liquid (a seed for the nucleus) atoms gradually form SRO, and this process increases the bond order. The change in order continues until most of the clustered atoms are crystalline. We assume a cubic fit to the free energy that shows that the dominant cubic term is of the form $Q_0\rho^2$ for possible free energy functional. A similar function was used for studying the comparison of bond order and density in the literature [85, 86].

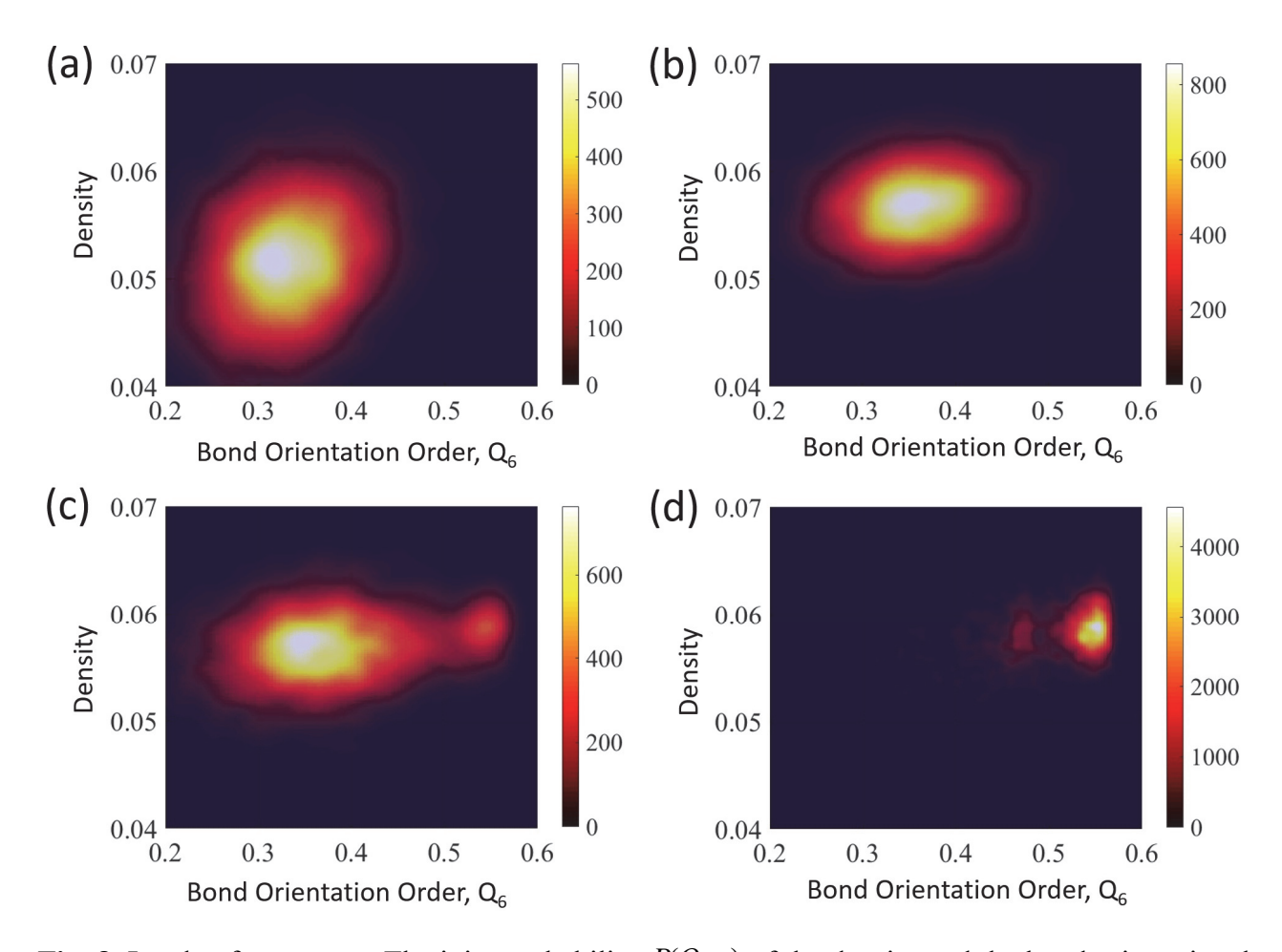


Fig. 8. Landau free energy. The joint probability $P(Q_6, \rho)$ of the density and the bond orientational order parameter is plotted for Al at 500 K at (a) 0 ps, (b) 90 ps, (c) 135 ps and (d) 180 ps.

As the interaction between density and bond order is quadratic in ρ and linear in Q_6 , the system can actually increase its bond orientational order parameters without affecting the translational order, but the contrary is not possible. This constrains the fluctuations towards a stronger increase in its orientational order. The interaction between the density and bond order also indicates a weak linear coupling between ρ^2 and Q_6 , which can be attributed to a low value of correlation coefficient (~0.20). This linear term also suggests that regions with a high orientational order will have a higher density on average than the other parts of the melt, which is consistent with our previous analysis in Figs. 5 and 6. As we observe in Fig. 8, there is a weak linear coupling between the bond-orientational order and the density, which ensures that fluctuations toward a higher density happen first then it directs towards higher orientational order parameters, meaning it forms the solid. From the joint probability of occurrence of Q_6 and ρ , as shown in Fig. 8, it can

be observed that the higher probability region gets extended along an axis as the time elapses. The slope of the joint probability distribution along the extended region reduces with increasing time step and it becomes almost parallel to the horizontal axis at 135 ps and 180 ps. Note that a higher slope indicates a high correlation between the parameters of the horizontal and vertical axis, while the parameters can be regarded as negligibly correlated as the slope becomes close to zero. This indicates a decaying correlation between density and bond orientation order in the system with elapsing time. The behavior of the joint probability is very similar for Fe and Mg as shown in Figs. S12 and S13, respectively, in the supplementary materials.

Based on the preceding discussions in the context of the heterogeneity in homogenous nucleation, it can be claimed that the ordering appears at the very early stage of the solidification while density increases. The increase in density brings the liquid atoms closer to each other creating amorphous SRO, and they can be also compared to glassy structures. The long-range crystalline order appears from the random fluctuations of the glassy structures in a highly dense environment. As shown in Fig. 8(a) in the initial liquid structure, the atoms have low $P(Q_6)$ and low $P(\rho)$. The atoms move towards a higher density region as the whole simulation box is being solidified. As the solidification proceeds, the number of atoms having higher $P(Q_6)$ gradually increases with a constant density, and this is evident by changes in the threshold of the colorbar in Fig. 8(b) (in a probabilistic framework), and at this intermediate stage, the SRO appears. These SRO can be designated as a part of the heterogeneity in homogenous nucleation. This heterogeneity exists later when the crystalline atoms form. As the solidification continues, the joint probability moves towards a higher Q_6 at a constant ρ (Fig. 8(c) and (d)). These steps for Fe and Mg (refer to Figs. S12 and S13 in the supplementary information) are similar to Al.

4. Conclusions

The homogenous nucleation during solidification from undercooled Al, Fe and Mg is studied by MD simulations utilizing the most accurate 2NN-MEAM interatomic potentials. MD simulations of homogenous nucleation predict formation of nuclei with bcc crystalline in Fe, fcc crystalline in Al, and hcp crystalline in Mg (see Figs. S4, S5, S7, S9 and S10 in the supplementary information). Al and Mg are always found to nucleate with stacking faults and TBs.

The TBs and GBs act as a catalyst to the nucleation process, as different orientations of the neighboring nuclei create a wetting angle and reduce the free energy of the nucleation. There is also clear evidence of purely heterogeneous nucleation during the homogenous nucleation process when an embryo forms on top of a previously formed solid nucleus. The heterogeneities were further explored by using bond order parameters for identifying SRO. Bond order parameter shows the intermediate non-crystalline solid phases which remain as heterogeneities during homogenous nucleation from a pure melt, regardless of the element type. It is found that the ico atoms are not precursors for formation of bcc-Fe nuclei, rather the SRO are responsible for forming the initial bcc-nuclei from Fe melt. Similar pathways are also found for fcc-Al and hcp-Mg, and all the fcc or hcp atoms form the random movement of SRO atoms at undercooled temperature. Overall, the process of crystallization from melt can be described in two stages. First, we observe the formation of supercooled dense liquid with bond orientational order indicating formation of SRO, which result in intermediate semi-ordered phases (crystalline and non-crystalline solids). In the next step the SRO transforms into long range crystalline phases.

The probability density function of bond order parameter $P(Q_6)$ indicates SRO when plotted against the density. The joint probability distribution of order parameter and density shows a weak linear coupling as the corresponding correlation coefficient is found to remain in a low range (~0.2). The joint probability also represents the Landau free energy functional, and accordingly the joint probability $P(Q_6, \rho)$ is assumed to be in the form of $Q_6\rho^2$. The interaction is quadratic in ρ and linear in Q_6 , meaning that the system can increase its orientational order without noticeably increasing the translational order. This constrains the fluctuations towards a stronger increase in its orientational order, resulting in large number of SRO atoms.

In the conventional/classical nucleation theory, the homogeneous nucleation does not consider any heterogeneity in the embryo; we have quantitatively shown that there are heterogeneities in the embryo and during homogeneous nucleation (no foreign materials) arising from heterogeneous liquid ordering or difference in orientations between two nuclei separated by a grain or twin boundary. Even though the embryo itself doesn't cause the heterogeneity during the homogeneous nucleation, the lower free energy at the twin/grain boundaries causes the embryo to form at the first place, indicate heterogeneity remains in homogeneous nucleation. In summary, our findings comprehensively confirm the evidence of heterogeneity in homogeneous nucleation during

Accepted in Journal of Materials Science and Technology 106 (2022) 77-89

solidification of different metals. The presence of SRO along with the primary crystalline phase can

be considered as heterogeneity in the homogenous nucleation of pure metals. In the later stages when

the initially formed critical nuclei grow in size, then embryo with different orientations or the

twin/stacking faults can be considered as the heterogeneity in homogenous nucleation. This paper

essentially looked into a fundamental aspect of solidification, the outcome of which is valid for a

wide range of pure metals. Solidification being an elementary aspect of a broad variety of

manufacturing techniques starting from metal casting to 3D printing, the inferences of this work

could be helpful for further developments in multiple relevant scientific areas.

Supplementary Materials

Supplementary Information accompanies this article on ().

Supplementary sections: Section 1 – Section 15

Supplementary figures: Figure S1 – Figure S13

Supplementary tables: Table S1 – Table S3

Acknowledgments

This study was financially supported by the National Science Foundation (Nos. NSF-CMMI

1855491 and NSF-CMMI 2031800). The authors are grateful for computer time allocation provided

by the Extreme Science and Engineering Discovery Environment (XSEDE), award number TG-

DMR 140008.

Author Contributions

Avik Mahata: Conceptualization, Methodology, Software, Formal analysis, Writing-Original draft

preparation. Tanmoy Mukhopadhyay: Methodology, Formal analysis, Writing-Reviewing and

Editing. Mohsen Asle Zaeem: Supervision, Conceptualization, Methodology, Formal analysis,

Writing-Original draft preparation, Funding Acquisition.

29

Data availability

All necessary data generated or analyzed during this study are included in this published article and the supplementary materials, and other auxiliary data are available from the corresponding author on reasonable request.

Competing interests

The authors declare no competing interests.

References

- [1] J.A. Dantzig, M. Rappaz, Solidification, EPFL press, 2009.
- [2] R. Asthana, A. Kumar, N.B. Dahotre, Materials processing and manufacturing science, Elsevier, 2006.
- [3] J.M. Howe, H. Saka, MRS bulletin 29 (2004) 951-957.
- [4] S.H. Oh, Y. Kauffmann, C. Scheu, W.D. Kaplan, M. Rühle, Science 310 (2005) 661-663.
- [5] T. Schülli, R. Daudin, G. Renaud, A. Vaysset, O. Geaymond, A. Pasturel, Nature 464 (2010) 1174-1177.
- [6] M. Gandman, Y. Kauffmann, C.T. Koch, W.D. Kaplan, Phys. Rev. Lett. 110 (2013) 086106.
- [7] N. Mauro, W. Fu, J. Bendert, Y. Cheng, E. Ma, K. Kelton, J. Chem. Phys. 137 (2012) 044501.
- [8] R. Dai, J.C. Neuefeind, D.G. Quirinale, K.F. Kelton, J. Chem. Phys. 152 (2020) 164503.
- [9] M. Xu, X. Ge, W. Yao, S. Tang, W. Lu, M. Qian, Y. Fu, H. Xie, T. Xiao, Q. Hu, Metall. Mater. Trans. A-Phys. Metall. Mater. Sci. 49 (2018) 4419-4423.
- [10] W. Yao, M. Xia, L. Zeng, X. Ge, M. Qian, Y. Wang, W. Lu, Y. Fu, H. Xie, T. Xiao, Metall. Mater. Trans. A-Phys. Metall. Mater. Sci. 50 (2019) 3441-3445.
- [11] S. Ma, A.J. Brown, R. Yan, R.L. Davidchack, P.B. Howes, C. Nicklin, Q. Zhai, T. Jing, H. Dong, Comm. Chem. 2 (2019) 1-12.
- [12] J. Zhao, Z. Tang, K. Kelton, C. Liu, P. Liaw, A. Inoue, X. Shen, S. Pan, M. Johnson, G. Chen, Intermetallics 82 (2017) 53-58.
- [13] X. Liu, J. Chem. Phys. 112 (2000) 9949-9955.
- [14] G. Neilson, M. Weinberg, J. Non-Cryst. Solids 34 (1979) 137-147.
- [15] D. Erdemir, A.Y. Lee, A.S. Myerson, Accounts Chem. Res. 42 (2009) 621-629.
- [16] G. Kahl, H. Löwen, J. Phys.-Condes. Matter 21 (2009) 464101.
- [17] S. Toxvaerd, J.Chem. Phys. 115 (2001) 8913-8920.
- [18] X. Sui, Y. Cheng, N. Zhou, B. Tang, L. Zhou, CrystEngComm 20 (2018) 3569-3580.
- [19] K. Oh, X.C. Zeng, J. Chem. Phys. 110 (1999) 4471-4476.
- [20] D. Srolovitz, G. Grest, M. Anderson, Acta Metall. Mater. 34 (1986) 1833-1845.
- [21] B. Böttger, J. Eiken, I. Steinbach, Acta Mater. 54 (2006) 2697-2704.
- [22] L. Gránásy, T. Börzsönyi, T. Pusztai, Phys. Rev. Lett. 88 (2002) 206105.
- [23] L. Gránásy, T. Pusztai, D. Saylor, J.A. Warren, Phys. Rev. Lett. 98 (2007) 035703.
- [24] L. Liu, S. Pian, Z. Zhang, Y. Bao, R. Li, H. Chen, Comput. Mater. Sci. 146 (2018) 9-17.
- [25] L. Gránásy, F. Podmaniczky, G.I. Tóth, G. Tegze, T. Pusztai, Chem. Soc. Rev. 43 (2014) 2159-2173.
- [26] Y. Shibuta, S. Sakane, T. Takaki, M. Ohno, Acta Mater. 105 (2016) 328-337.
- [27] M. Finnis, J. Sinclair, Philos. Mag. 50 (1984) 45-55.
- [28] T. Kawasaki, H. Tanaka, Proc. Natl. Acad. Sci. 107 (2010) 14036-14041.
- [29] E. Asadi, M. Asle Zaeem, S. Nouranian, M.I. Baskes, Phys. Rev. B 91 (2015) 024105.
- [30] Y.-M. Kim, N.J. Kim, B.-J. Lee, Calphad 33 (2009) 650-657.

- [31] S. Kavousi, B.R. Novak, M. Asle Zaeem, D. Moldovan, Comput. Mater. Sci. 163 (2019) 218-229.
- [32] D. Faken, H. Jónsson, Comput. Mater. Sci. 2(2) (1994) 279-286.
- [33] P.J. Steinhardt, D.R. Nelson, M. Ronchetti, Phys. Rev. B 28(2) (1983) 784.
- [34] W.C. Swope, H.C. Andersen, Phys. Rev. B 41 (1990) 7042.
- [35] A. Mahata, M. Asle Zaeem, Comput. Mater. Sci. 163 (2019) 176-185.
- [36] A. Mahata, M. Asle Zaeem, J. Cryst. Growth 527 (2019) 125255.
- [37] A.K. Mahata, M. Asle Zaeem, Model. Simul. Mater. Sci. Eng. 28 (2019) 019601.
- [38] A. Mahata, M. Asle Zaeem, M.I. Baskes, Model. Simul. Mater. Sci. Eng. 26 (2018) 025007.
- [39] A. Mahata, M. Asle Zaeem, Insights on Solidification of Mg and Mg–Al Alloys by Large Scale Atomistic Simulations, Magnesium Technology 2020, Springer, 2020, pp. 51-53.
- [40] B.-J. Lee, M. Baskes, Phys. Rev. B 62 (2000) 8564.
- [41] B.-J. Lee, M. Baskes, H. Kim, Y.K. Cho, Second nearest-neighbor modified embedded atom method potentials for bcc transition metals, Phys. Rev. B 64 (2001) 184102.
- [42] E. Asadi, M. Asle Zaeem, S. Nouranian, M.I. Baskes, Acta Mate. 86 (2015) 169-181.
- [43] E. Asadi, M. Asle Zaeem, Acta Mate. 107 (2016) 337-344.
- [44] M. Asadian Nozari, R. Taghiabadi, M. Karimzadeh, M. Ghoncheh, J. Mater. Sci. Technol. 31 (2015) 506-512.
- [45] E. Lee, K.-R. Lee, M. Baskes, B.-J. Lee, Phys. Rev. B 93 (2016) 144110.
- [46] A. Mahata, M. Asle Zaeem, Model. Simul. Mater. Sci. Eng. 27 (2019) 085015.
- [47] W. Lechner, C. Dellago, J. Chem. Phys. 129 (2008) 114707.
- [48] T. Aste, M. Saadatfar, T. Senden, Phys. Rev. E 71(6) (2005) 061302.
- [49] Y. Shibuta, S. Sakane, E. Miyoshi, S. Okita, T. Takaki, M. Ohno, Nature Communications 8(1) (2017) 10.
- [50] A. Mahata, M. Asle Zaeem, M.I. Baskes, Understanding homogeneous nucleation in solidification of aluminum by molecular dynamics simulations, Model. Simul. Mater. Sci. Eng. 26(2) (2018) 025007.
- [51] S. Auer, D. Frenkel, Nature 409 (2001) 1020-1023.
- [52] V. Kalikmanov, Classical nucleation theory, Nucleation theory, Springer, 2013, pp. 17-41.
- [53] J.W. Schmelzer, Nucleation theory and applications, John Wiley & Sons, 2006.
- [54] I. Gutzow, J. Schmelzer, The vitreous state, Springer, 1995.
- [55] A. Myerson, Handbook of industrial crystallization, Butterworth-Heinemann, 2002.
- [56] K. Kelton, Solid state Phys. 45 (1991) 75-177.
- [57] V.M. Fokin, E.D. Zanotto, N.S. Yuritsyn, J.W. Schmelzer, J. Non-Cryst. Solids 352 (2006) 2681-2714.
- [58] W. Pan, A.B. Kolomeisky, P.G. Vekilov, J. Chem. Phys. 122 (2005) 174905.
- [59] S. Sen, T. Mukerji, J. Non-Cryst. Solids 246 (1999) 229-239.
- [60] Z. Lin, E. Leveugle, E.M. Bringa, L.V. Zhigilei, J. Phys. Chem. C 114 (2010) 5686-5699.
- [61] X.-M. Bai, M. Li, J. Chem. Phys. 124 (2006) 124707.
- [62] D. Turnbull, J. Appl. Phy. 21 (1950) 1022-1028.
- [63] Z. Jian, K. Kuribayashi, W. Jie, Mater. Trans. 43 (2002) 721-726.
- [64] T. Frolov, Y. Mishin, J. Chem. Phys. 131 (2009) 054702.
- [65] X. Wang, R.G. Guan, N. Guo, Z.Y. Zhao, Y. Zhang, N. Su, J. Mater. Sci. Technol. 32 (2016) 154-163.
- [66] S.D. Panfilis, A. Filipponi, J. Appl. Phys. 88 (2000) 562-570.
- [67] C.G. Levi, R. Mehrabian, Microstructures of rapidly solidified aluminum alloy submicron powders, Metall. Trans. A 13 (1982) 13-23.
- [68] L.-Y. Chen, J.-Q. Xu, H. Choi, M. Pozuelo, X. Ma, S. Bhowmick, J.-M. Yang, S. Mathaudhu, X.-C. Li, Nature 528 (2015) 539-543.
- [69] Z. Hou, Z. Tian, R. Liu, K. Dong, A. Yu, Comput. Mater. Sci. 99 (2015) 256-261.
- [70] P.M. Larsen, S. Schmidt, J. Schiøtz, Model. Simul. Mater. Sci. Eng. 24 (2016) 055007.
- [71] A. Stukowski, Model. Simul. Mater. Sci. Eng. 18(1) (2009) 015012.
- [72] V. Dubrovskii, Fundamentals of Nucleation Theory, Nucleation Theory and Growth of Nanostructures, Springer, 2014, pp. 1-73.

- [73] B. Chalmers, Principles of solidification, Applied solid state physics, Springer, 1970, pp. 161-170.
- [74] D.L. Olmsted, S.M. Foiles, E.A. Holm, Acta Mater. 57 (2009) 3694-3703.
- [75] M. Gündüz, J.D. Hunt, Acta Metall. 37 (1989) 1839-1845.
- [76] H. Zhang, M. Upmanyu, D. Srolovitz, Mater. 53 (2005) 79-86.
- [77] G. Lu, N. Kioussis, V.V. Bulatov, E. Kaxiras, Phys. Rev. B 62 (2000) 3099-3108.
- [78] B. Hammer, K.W. Jacobsen, V. Milman, M.C. Payne, J. Phys.-Condes. Matter 4 (1992) 10453-10460.
- [79] D. Wolf, Philos. Mag. 62 (1990) 447-464.
- [80] J.L. Nilles, D.L. Olson, J. Appl. Phys. 41 (1970) 531-532.
- [81] P. Bristowe, A. Crocker, Philos. Mag. 31 (1975) 503-517.
- [82] R.L. Fleischer, Scr. Metall. 20 (1986) 223-224.
- [83] T. Schilling, H.J. Schöpe, M. Oettel, G. Opletal, I. Snook, Phys. Rev. Lett. 105 (2010) 025701.
- [84] H. Tanaka, Eur. Phys. J. E 35 (2012) 113.
- [85] J. Russo, H. Tanaka, J. Chem. Phys. 145 (2016) 211801.
- [86] J. Russo, H. Tanaka, in: AIP Conference Proceedings, AIP, 2013, pp. 232-237.